

PAPER • OPEN ACCESS

Modelling of magnetoelectric nanoparticles for non-invasive brain stimulation: a computational study

To cite this article: Serena Fiocchi *et al* 2022 *J. Neural Eng.* **19** 056020

View the [article online](#) for updates and enhancements.

You may also like

- [High inductance magnetic-core coils have enhanced efficiency in inducing suprathreshold motor response in rats](#)
Hieu Nguyen, Sergey N Makaroff, Charlotte Qiong Li *et al.*
- [Novel TMS coils designed using an inverse boundary element method](#)
Clemente Cobos Sánchez, Jose María Guerrero Rodríguez, Ángel Quirós Olozábal *et al.*
- [Review on biophysical modelling and simulation studies for transcranial magnetic stimulation](#)
Jose Gomez-Tames, Ilkka Laakso and Akimasa Hirata



Breath Biopsy Conference 5th & 6th November Online

Join the conference to explore the **latest challenges** and advances in **breath research**, you could even **present your latest work!**

Register now for free!

BREATH BIOPSY

- Main talks
- Early career sessions
- Posters

The banner features a dark background with orange accents. It includes the conference title, dates, and a call to action. A central image shows a group of people, and a list of activities is provided on the right side.



PAPER

OPEN ACCESS

RECEIVED

23 December 2021

REVISED

1 September 2022

ACCEPTED FOR PUBLICATION

8 September 2022

PUBLISHED

23 September 2022

Original content from this work may be used under the terms of the [Creative Commons Attribution 4.0 licence](#).

Any further distribution of this work must maintain attribution to the author(s) and the title of the work, journal citation and DOI.



Modelling of magnetoelectric nanoparticles for non-invasive brain stimulation: a computational study

Serena Fiocchi* , Emma Chiaramello , Alessandra Marrella , Marta Bonato , Marta Parazzini and Paolo Ravazzani

CNR Consiglio Nazionale delle Ricerche, Istituto di Elettronica e di Ingegneria dell'Informazione e delle Telecomunicazioni IEIIT, 10129 Turin, Italy

* Author to whom any correspondence should be addressed.

E-mail: serena.fiocchi@ieiit.cnr.it

Keywords: magnetoelectric nanoparticles, brain stimulation, computational modelling

Abstract

Objective. Recently developed magnetoelectric nanoparticles (MENPs) provide a potential tool to enable different biomedical applications. They could be used to overcome the intrinsic constraints posed by traditional neurostimulation techniques, namely the invasiveness of electrodes-based techniques, the limited spatial resolution, and the scarce efficiency of magnetic stimulation. **Approach.** By using computational electromagnetic techniques, we modelled the behaviour of recently designed biocompatible MENPs injected, in the shape of clusters, in specific cortical targets of a highly detailed anatomical head model. The distributions and the tissue penetration of the electric fields induced by MENPs clusters in each tissue will be compared to the distributions induced by traditional transcranial magnetic stimulation (TMS) coils for non-invasive brain stimulation positioned on the left prefrontal cortex (PFC) of a highly detailed anatomical head model. **Main results.** MENPs clusters can induce highly focused electric fields with amplitude close to the neural activation threshold in all the brain tissues of interest for the treatment of most neuropsychiatric disorders. Conversely, TMS coils can induce electric fields of several tens of $V\ m^{-1}$ over a broad volume of the PFC, but they are unlikely able to efficiently stimulate even small volumes of subcortical and deep tissues. **Significance.** Our numerical results suggest that the use of MENPs for brain stimulation may potentially led to a future pinpoint treatment of neuropsychiatric disorders, in which an impairment of electric activity of specific cortical and subcortical tissues and networks has been assumed to play a crucial role.

1. Introduction

The last years have experienced an unprecedented growth of nanomedicine applications (Pelaz *et al* 2017, Bayda *et al* 2019), boosted by the progress in nanotechnology and the parallel interest in highly personalized precision medicine (Goetz and Schork 2018). Among the various nanotechnology enablers recently introduced in the biomedical field, such as ferromagnetic super paramagnetic iron oxide nanoparticles, metallic and polymeric nanoparticles (Ali *et al* 2016, Banik *et al* 2016, Lee and Jun 2019), magneto electric nanoparticles (MENPs) have gained attention for their unique properties.

The most widely used type of MENPs are core shell 'magneto electric' (ME) nanostructures, made of a ferromagnetic core and a ferroelectric shell. Due

to their multiferroic physics they exhibit the so-called 'ME effect', which raises from the strain mediated coupling between the magnetostrictive properties of the core and the piezoelectric properties of the shell (Fiebig 2005, Eerenstein *et al* 2006). The ME effect then provides MENPs the capability to efficiently convert the magnetic energy that reach them, into electric energy (Kopyl *et al* 2021).

On a practical ground, MENPs can wirelessly induce strong localized electric fields when properly activated with magnetic fields. That feature makes them suitable for a great number of biomedical applications, where the wireless control of the cellular-electric field interactions plays a crucial role (Ryan *et al* 2021). Very early applications of MENPs include local nervous system electric stimulation (Guduru *et al* 2015, Singer *et al* 2020, Kozielski

et al 2021, Nguyen *et al* 2021), targeted drug delivery (Xie *et al* 2008, Guduru *et al* 2013, Chen *et al* 2017, Kaushik *et al* 2017, Stimphil *et al* 2017, Stewart *et al* 2018), also across the blood–brain barrier (Barbu *et al* 2009, Nair *et al* 2013, Kaushik *et al* 2016, Rodriguez *et al* 2017), and high contrast bioimaging (Nagesetti *et al* 2017, Guduru *et al* 2018). Systematic review studies of current and potential biomedical applications of MENPs can be found in (Golovin *et al* 2017, Kopyl *et al* 2021, Kolishetti *et al* 2022).

Among these applications, wireless MENPs-based brain stimulation could represent a valuable alternative to modern brain stimulation approaches, whose capabilities are limited by either their invasiveness, as for deep brain stimulation (DBS) (McIntyre *et al* 2004) and intracortical micro-stimulation (ICMS) (Bak *et al* 1990), or the low efficacy and poor spatial resolution as for transcranial magnetic stimulation (TMS) (Loo and Mitchell 2005).

The idea of using MENPs for the central nervous system stimulation was first proposed by (Yue *et al* 2012) in a computational study in which small size core–shell CoFe_2O_4 – BaTiO_3 MENPs, injected in the area of the subthalamic nucleus of a model patient with Parkinson's disease (PD), were exposed to a low magnetic field (below 80 kA m^{-1}) at 80 Hz to induce high electric fields (amplitude $> 10^5 \text{ V m}^{-1}$). These electric fields were theoretical proven to be effective in bringing the electric activity of the impaired target brain structures of the PD patient to levels comparable to healthy people.

However, only recently this proof of concept has been corroborated with some experimental results (Guduru *et al* 2015, Kozielski *et al* 2021, Nguyen *et al* 2021). (Guduru *et al* 2018) demonstrated the effective capability of MENPs to modulate the brain electroencephalography (EEG) activity *in vivo* when activated with a low-energy (i.e. around 8000 A m^{-1}) AC magnetic field in the 0–20 Hz frequency range. Very recently, (Kozielski *et al* 2021) implanted similar MENPs directly in the brain tissue by using stereotactic injection into the subthalamic region of mice. Interestingly, a DC magnetic field of 220 mT was coupled with a small AC field (6 mT, 140 Hz) to induce a local neural activity that was able to activate regions of the corticobasal ganglia-thalamocortical circuit, showing the efficacy of the wireless activation of MENPs for deep brain stimulation. In parallel, in (Nguyen *et al* 2021), authors reported a cortical activation of individual neuron and large neural networks *in vivo* by activating MENPs with two electromagnets ($\sim 500 \text{ ms}$ pulse-width at ~ 30 – 40 kA m^{-1}), further proving the potential of CoFe_2O_4 – BaTiO_3 MENPs to interact with neural activities at magnetic field intensities much lower than those used for typical TMS protocols (Deng *et al* 2014, Gorelick *et al* 2014), i.e. up to 1–2 T around the coil loop equivalent, in the vacuum, to 800–1600 kA m^{-1} .

To provide significant insights into these experimental observations and to boost the translation of this approach in clinic, computational modelling becomes an imperative component (Hu *et al* 2017) that, to date, is still scarcely applied to this research field.

Moreover, since in this paper we focus on the specific possible application of MENPs mediated electric stimulation of different cortical and subcortical targets for the non-invasive treatment of neuropsychiatric disorders, computational models represent the only way to assess the electric fields in target tissues, most of which are located deep in the brain.

Neurological and psychiatric disorders share indeed a dysfunction of both cortical and deep brain areas which translates in a partial alteration of the corresponding brain target electric activity (Johnson *et al* 2013). To restore these brain functions methods based on the direct application of electric field in the brain, such as DBS and ICMS, require the implant of electrodes in the tissue to be stimulated, resulting in all side effects due to their intrusiveness. On the other hand, non-invasive brain stimulation techniques based on electromagnetic fields have been successfully used to this purpose (for a review see (Brunoni *et al* 2019)), thus proving that the activation/inhibition of electric patterns, even when non-invasively administered, could be a valuable treatment option to the classical pharmacological therapy.

Among the others, non-invasive repetitive TMS (rTMS) has been proposed as the main tool for the non-pharmacological treatment of different psychiatric disorders, specifically granting FDA-clearance to treat major depression in 2008, followed by migraine headaches in 2013, obsessive compulsive disorders in 2018, smoking addiction in 2020 (Regenold *et al* 2022). However, even if largely used, the rTMS approach showed some limits in reaching specific deep subcortical networks involved in the progression of most of neuropsychiatric disorders (Demirtas-Tatlidede *et al* 2013). The possibility of using CoFe_2O_4 – BaTiO_3 MENPs, once positioned semi-invasively in the selected brain targets, for treating these types of disorders could represent a disruptive novelty in clinical practice, being a substantial improvement in terms of electric field penetration and focusing capability over the currently used rTMS approaches.

This study, therefore, precisely addresses this possibility.

Specifically, the behaviour of clusters of CoFe_2O_4 – BaTiO_3 MENPs, already characterized in literature, will be modelled in specific cortical targets of a highly detailed anatomical head model. The distributions and the tissue penetration of the electric field induced by MENPs will be compared to the distributions induced by traditional TMS coils used for the treatment of neuropsychiatric disorders

(Deng *et al* 2014, Gorelick *et al* 2014, Regenold *et al* 2022), namely figure-of-eight (FoE) TMS coils positioned on the left prefrontal cortex (PFC).

2. Material and methods

The methodology here applied to model the electric field (E) distributions induced by both MENPs and FoE coils, is similar to the one described in previous papers (see, e.g. Parazzini *et al* 2017, Fiocchi *et al* 2018). In summary, the E distributions were estimated using the simulation platform SIM4life (by ZMT Zurich Med Tech AG, Zurich, Switzerland, www.zurichmedtech.com) and a highly detailed human head anatomical model (Iacono *et al* 2015). Details about how MENPs and TMS coil were modelled, about the brain regions considered, the numerical methods used to estimate the E distributions and the analysis of results are reported in the following.

2.1. Human model

A multimodal imaging-based anatomical model, named MIDA (Iacono *et al* 2015) (see figure 1), of the head and neck of one healthy 29 years old female volunteer, segmented and reconstructed from three different magnetic resonance imaging (MRI) modalities at a 500 μm isotropic resolution was used in this study. The head model distinguishes a total of 153 different regions, involving a high number of brain structures. Since this study aims evaluating the induced E amplitude distributions in the brain regions of the limbic system involved in the reward-related pathways, different structures, both cortical and deep, were considered as target tissues, similarly to the strategy followed by previous studies (Parazzini *et al* 2017, Fiocchi *et al* 2018). As to the cortical areas, the PFC, the dorsolateral PFC (DLPFC), medial PFC (MPFC), cingulate cortex and insula regions were identified by means of a brain atlas (Harnsberger and Macdonald 2006) as they were not specifically segmented in the model used (see figure 1(c)). As to the deep structures, amygdala, hippocampus, hypothalamus, mammillary body, nucleus accumbens and ventral tegmental area were considered (see figure 1(d)). The E field distributions were analysed in the left part of all the brain structures with a symmetry in the two hemispheres. The dielectric properties of each tissue have been assigned according to literature data (IT'IS Foundation 2018) at the MENPs AC field and TMS single pulse frequency, i.e. 140 Hz (Kozielski *et al* 2021) and 5 kHz (Deng *et al* 2014), respectively.

2.2. MENPs cluster model

MENPs, thanks to their chemical composition, exhibit a strong coupling between magnetic and electric field, thus enabling to induce locally E fields when wireless stimulated with low-amplitude magnetic

fields (Eerenstein *et al* 2006). This behaviour is quantified by the magneto-electric coefficient α , defined by:

$$\alpha = \frac{\Delta E}{\Delta H} \quad (1)$$

where E is induced electric field, and H is the applied magnetic field.

According to literature, commonly experimental values of particulate magnetoelectric composites such as MENPs are in the range of 0.01–0.1 $\text{V cm}^{-1} \text{Oe}^{-1}$ (corresponding to 0.0125–0.125 V A^{-1}) (Liu *et al* 2005, Devan and Chougule 2007, Grössinger *et al* 2008). To simulate the presence of MENPs as sources of E fields for brain stimulation, they were modelled as spherical agglomerates (in the following ‘clusters’) with radius equal to 1 mm. This approach corresponds to the experimental procedure of a recent study (Kozielski *et al* 2021), in which the authors injected MENPs into the subthalamic region of mice and determined that they occupied a volume comparable to their rodent DBS electrodes. We hypothesized to inject a single MENPs cluster in the centre of each tissue here identified as target of the stimulation and that it occupied a volume comparable to a human DBS electrode. Table 1 shows the volume of each cortical and deep region of interest, and the percentage of the volume of the region occupied by one MENPs cluster. Then, to assess the influence of multiple injection sites in each cortical region on the E field distributions, we also performed simulations with two MENPs clusters and four MENPs clusters. The positions of the MENPs clusters inside each region were defined assuring that each cluster was surrounded by the tissue of interest and that the relative distance between clusters was large enough to avoid reciprocal influence (i.e. the electric field generated by each cluster is close to 0 in correspondence with other clusters). For the deep brain structures, due to their smaller volume, only one single MENPs cluster and two MENPs clusters were modelled. Their positions were defined based on the same criteria established for the cortical region clusters.

The ME effect, elicited in (Kozielski *et al* 2021) by superimposing 220 mT DC and 3 mT AC magnetic fields at a frequency of 140 Hz, was here modelled by assuming that the maximum magnetic field produced by external DC and AC systems reached the nanoparticles, wherever positioned, and then by setting a uniform potential on the cluster surface. This boundary condition has been chosen as the most general and appropriate to mimic the macroscopic electric behaviour of a MENPs cluster when the exact configuration of single MENPs inside the cluster and of the B -field lines along which the single MENPs align are not known, as in the present study. Specifically, MENPs clusters were modelled as spherical charged wireless electrodes with surface potential tuned to obtain a maximum E amplitude

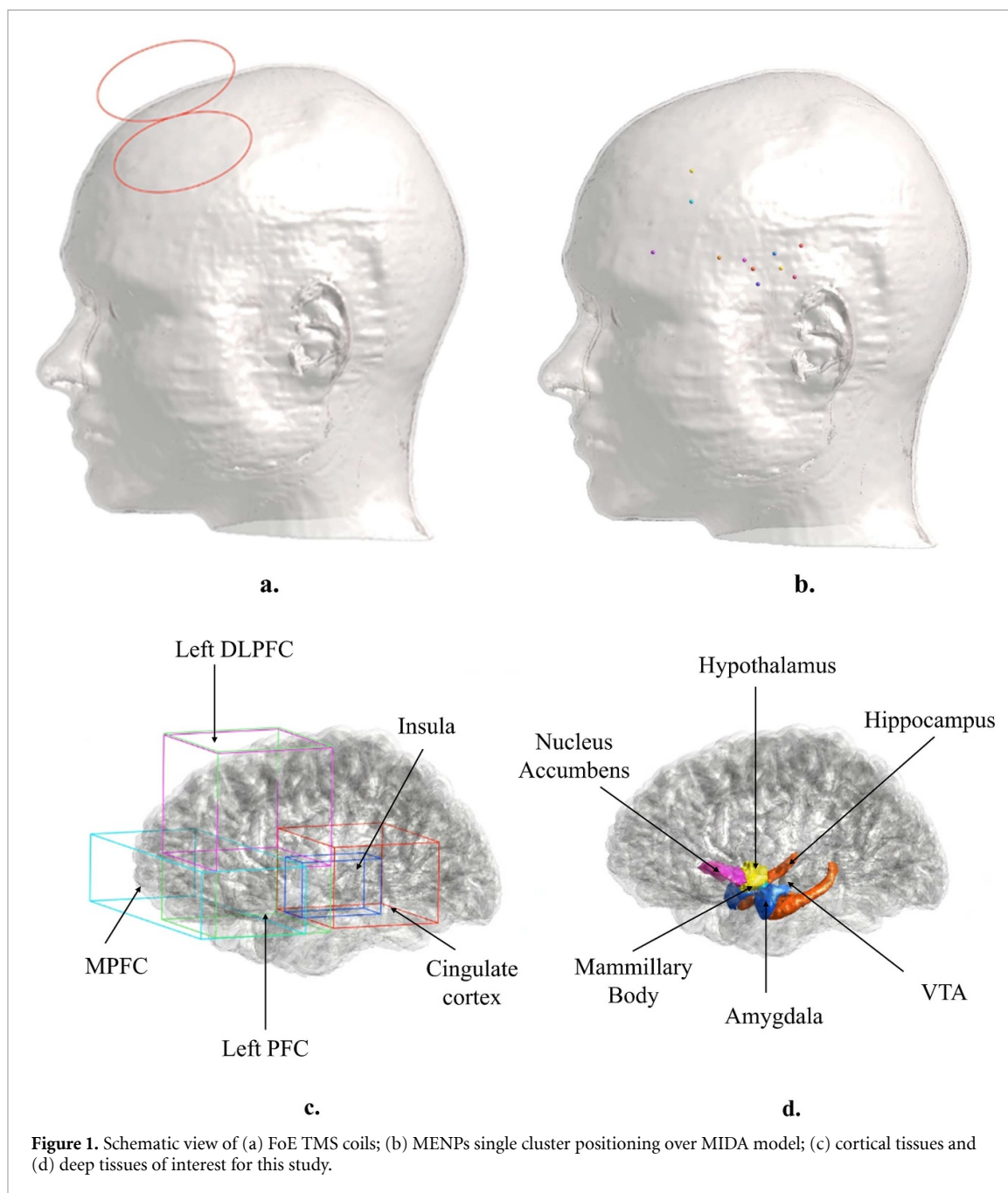


Figure 1. Schematic view of (a) FoE TMS coils; (b) MENPs single cluster positioning over MIDA model; (c) cortical tissues and (d) deep tissues of interest for this study.

equal to 100 V m^{-1} on the left PFC. This threshold is commonly acknowledged, in TMS computational studies, as the cortical motor threshold and then here intended as the ‘neural activation threshold’ (Danner *et al* 2012). This approach resulted in a potential of amplitude equals to 92.7 mV on each cluster surface, and a corresponding magneto-electric coefficient α of $0.0155 \text{ V cm}^{-1} \text{ Oe}^{-1}$ (i.e. 0.0194 V A^{-1}), which is in the range of previously measured ME coefficients of similar $\text{CoFe}_2\text{O}_4\text{-BaTiO}_3$ NP (i.e. from 0.01 to over $0.1 \text{ V cm}^{-1} \text{ Oe}^{-1}$) (Liu *et al* 2005, Devan and Chougule 2007, Grössinger *et al* 2008, Kopyl *et al* 2021).

Also, in the case of simultaneous presence of more than one cluster, the amplitude of the potential on each cluster was imposed to be equal to 92.7 mV.

2.3. TMS coil model

The E amplitude distributions in the various brain regions due to the MENPs have been compared with the one induced by the classical FoE, which is the first FDA-approved rTMS systems for the treatment of major depressive disorder. This system allows a precise and focal stimulation of cortical regions, including the main target for depressive disorders treatment (i.e. PFC and DLPFC). Here (see figure 1(a)), it has been modelled as two adjacent current paths, with dimensions based on published data (Parazzini *et al* 2017, Fiocchi *et al* 2018). Specifically, it is composed by two planar circular windings of 70 mm diameter, placed tangentially to the head and pointing 45° away from the anterior–posterior axis, as reported in experimental studies (see, e.g. Roth *et al* 2007, Deng *et al*

Table 1. Volume of each cortical and deep brain region of interest and percentage of it occupied by one MENPs cluster.

| | | Total volume (cm ³) | Percentage of volume occupied by MENPs |
|---------------------|----------------------|------------------------------------|--|
| Cortical regions | Cingulate cortex | 33.89 | 0.01 |
| | DLPFC | 31.99 | 0.01 |
| | Insula | 9.62 | 0.04 |
| | MPFC | 54.37 | 0.01 |
| | PFC | 62.93 | 0.01 |
| Deep regions | Amygdala | 1.46 | 0.29 |
| | Hippocampus | 2.49 | 0.17 |
| | Hypothalamus | 0.99 | 0.43 |
| | Mammillary body | 0.15 | 2.83 |
| | Nucleus accumbens | 0.45 | 0.92 |
| | VTA | 0.60 | 0.70 |

2013). The point where the two windings are in contact was posed at 5 cm anteriorly to the motor cortex region corresponding to the abductor pollicis brevis of the hand, on the left hemisphere, for targeting the left PFC. The minimum spacing between the coil and the surface of the head model was about 10 mm to account for the thickness of the coil insulation not included in the model. The current flows in opposite directions in the two windings, at the fundamental frequency of 5 kHz, which is representative of efficient TMS pulses (Deng *et al* 2014). Following the strategies of previous studies, the current intensity delivered was set equal to about 8 kA to obtain on the left PFC an E distribution with maximum amplitude equal to the neural activation threshold, i.e. 100 V m⁻¹ (Danner *et al* 2012).

2.4. Numerical methods

Two different solvers implemented on the simulation platform SIM4life (by ZMT Zurich Med Tech AG, Zurich, Switzerland, www.zurichmedtech.com) were used to quantify the E amplitude distributions in tissues.

When simulating MENPs clusters, here modelled as spherical electrodes working in the near-DC frequency range (Kaushik *et al* 2017, Kozielski *et al* 2021, Nguyen *et al* 2021), the ohmic quasi static approximation was used. The electric potential (φ) was obtained by solving the Laplace equation through a finite element method:

$$\nabla \cdot (\sigma \nabla \varphi) = 0 \quad (2)$$

where σ (S m⁻¹) is the electrical conductivity of tissues. In the low frequency approximation adopted, ohmic currents dominate displacement currents and capacitive effects are disregarded. The electric field

(E) distributions were obtained by means of the following relation:

$$E = -\nabla \varphi. \quad (3)$$

When considering the FoE coil, the magneto quasi-static approximation was used, which uses a Biot–Savart solver based on the scalar potential finite element method. In the low frequency range the magnetic vector potential A is decoupled from E . E can be derived from the scalar potential φ , which is given by:

$$-\nabla \cdot \sigma \nabla \varphi = j\omega \nabla \cdot (\sigma A) \quad (4)$$

where σ is the tissue conductivity and ω is the angular frequency of the field. In this approximation tissues are considered as purely resistive, thus disregarding their dielectric dispersion. A is calculated using the Biot–Savart’s law whereas the finite element method is used to solve for φ .

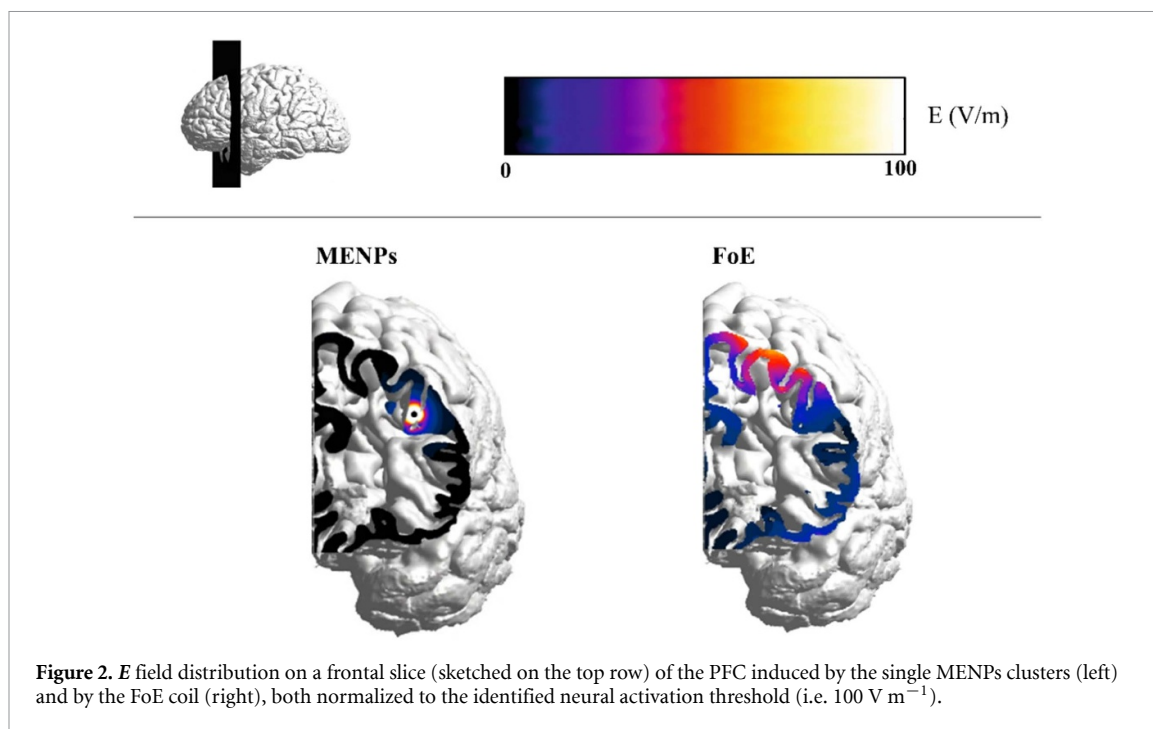
A non-uniform hexahedral mesh, with a minimum mesh step equals to 0.1 mm and 0.4 mm for MENPs and FoE simulations, respectively, was applied to the computational domain, thus allowing to discretize the thinnest structures of the model.

2.5. Data analysis

The E distributions induced by MENPs and by the FoE coil placed to target the PFC were evaluated both in terms of spread and magnitude, when the amplitude of the potential imposed on MENPs surface and the intensity of the current circulating in the coil were high enough to obtain a maximum E field amplitude of 100 V m⁻¹ on the left PFC. The spread of the E amplitude distributions in each of brain region target of the stimulation was quantified as the volume percentage of these brain regions with an E amplitude equals or greater than 1, 10, 50 and 70 V m⁻¹, corresponding to 1%, 10%, 50% and 70% of the maximum amplitude of E in the PFC. We will use V1, V10, V50 and V70 to identify these volume percentages. This analysis quantifies the spread of the E amplitude distribution inside each brain region of interest, since these parameters provide a quantification of the ability of the different sources to focalize specific E amplitude values in a small volume.

To describe the amplitude of the induced E fields, the descriptive statistics of the E amplitude distributions (i.e. min, 25th, 50th, 75th percentiles and maximum of the distribution) were calculated in each brain region of interest for the treatment of depression.

A non-parametric Kruskal–Wallis test was applied to test the influence of using different number of MENPs clusters or the FoE on the E amplitude distribution extracted in each area of interest. Values of $p < 0.05$ were considered as statistically significant.



3. Results

The analysis of the results will be presented considering separately cortical and subcortical regions.

3.1. Electric field distribution on the brain cortex

Figure 2 shows, as an example, the E field amplitude, a single MENPs cluster (left) and by the FoE coil (right) both normalized to the neural activation threshold (i.e. $E = 100 \text{ V m}^{-1}$).

It can be noted that MENPs cluster can induce over the left PFC a very focused distribution which decays very sharply few millimetres away from the cluster itself. On the contrary, FoE induces below its centre a broad E field distribution, characterized by values higher than 50 V m^{-1} (colourmap from orange to white) over a consistent portion of the shown cortical section. These considerations are more precisely quantified by figure 3, which shows the descriptive statistics (minimum, 25th, 50th, 75th and maximum) of the E amplitude distributions induced by the three MENPs configurations and by the FoE coil in the cortical regions of interest. From figures 3(a)–(c) it can be observed that, whatever the MENPs are positioned, they can stimulate the neural tissue (top whiskers everywhere approach the activation threshold). However, a strong decay of the other percentiles can be observed, with the 50th percentile staying always below 1 V m^{-1} , regardless the cortical region considered and the number of clusters. The number of clusters injected in each area influences the E amplitude distributions, with an increase of the median values across the cortical areas when increasing the number of MENPs clusters. When considering figure 3(d), results show that FoE can induce

E fields close to the neural activation threshold only in correspondence of the cortical area where is placed, i.e. PFC and DLPFC, but can invest with E amplitudes higher than few V m^{-1} more than the 75% of all the target tissues.

The observed differences between the E amplitude distributions obtained by MENPs clusters and FoE are confirmed as statistically significant by the Kruskal–Wallis test.

Those differences in focusing capability are further quantified by the V_x reported in table 2. FoE coil can indeed induce very low levels of E field (up to 1% of the activation threshold equals to 1 V m^{-1}) in almost the entire volume of each tissue of interest and can invest with E field up to 10 V m^{-1} a significant volume of the DLPFC, with a low spatial resolution. Conversely, MENPs are effective in stimulating only a very small percentage of tissues volume, with a slight increasing trend as increasing the number of MENPs clusters, almost doubling the volumes activated when the cluster number doubles.

That would also mean that the computed percentages can be enlarged through an accurate strategy of MENPs positioning and by calibrating the administered dose to stimulate specific areas.

3.2. Electric field distribution on the deep tissue

Figure 4 shows, as an example, the E field distribution on the surface of the target deep structures induced by the single MENPs clusters (left) and by the FoE coil (right).

Colourmaps maxima are limited, for the sake of readability, to 10 V m^{-1} . As expected, even in these regions, MENPs generate E field at the neural activation threshold around the cluster and can invest a

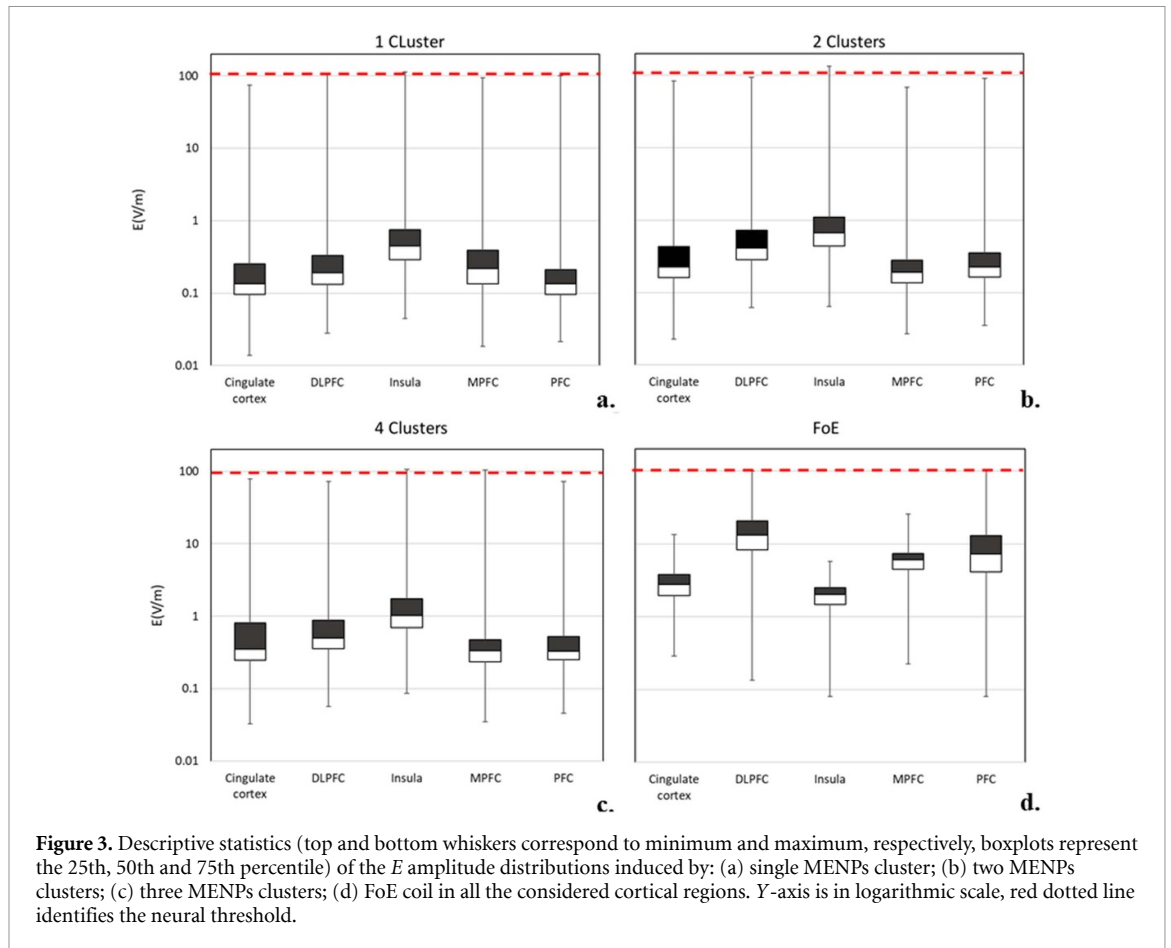


Figure 3. Descriptive statistics (top and bottom whiskers correspond to minimum and maximum, respectively, boxplots represent the 25th, 50th and 75th percentile) of the E amplitude distributions induced by: (a) single MENPs cluster; (b) two MENPs clusters; (c) three MENPs clusters; (d) FoE coil in all the considered cortical regions. Y-axis is in logarithmic scale, red dotted line identifies the neural threshold.

Table 2. Percentage volume of each cortical region with E amplitude higher than 1%, 10%, 50% and 70% (V1, V10, V50, V70, respectively) of the maximum amplitude of E in the PFC for each stimulation configuration.

| | | Cingulate cortex | DLPFC | Insula | MPFC | PFC |
|-----------|-----|------------------|-------|--------|-------|-------|
| 1 Cluster | V1 | 6.9 | 4.6 | 16.5 | 7.0 | 2.1 |
| | V10 | 0.2 | 0.2 | 0.9 | 0.1 | 0.1 |
| | V50 | < 0.1 | < 0.1 | < 0.1 | < 0.1 | < 0.1 |
| | V70 | < 0.1 | < 0.1 | < 0.1 | < 0.1 | < 0.1 |
| 2 Cluster | V1 | 11.9 | 14.2 | 28.5 | 6.0 | 4.7 |
| | V10 | 0.4 | 0.2 | 1.4 | 0.3 | 0.2 |
| | V50 | < 0.1 | < 0.1 | < 0.1 | < 0.1 | < 0.1 |
| | V70 | < 0.1 | < 0.1 | < 0.1 | < 0.1 | < 0.1 |
| 4 Cluster | V1 | 20.0 | 20.4 | 51.2 | 9.6 | 7.0 |
| | V10 | 0.5 | 0.3 | 2.0 | 0.3 | 0.3 |
| | V50 | < 0.1 | < 0.1 | < 0.1 | < 0.1 | < 0.1 |
| | V70 | < 0.1 | < 0.1 | < 0.1 | < 0.1 | < 0.1 |
| FoE | V1 | 97.5 | 99.7 | 90.8 | 100 | 98.7 |
| | V10 | < 0.1 | 64.7 | < 0.1 | 3.9 | 33.4 |
| | V50 | < 0.1 | 0.3 | < 0.1 | < 0.1 | 0.1 |
| | V70 | < 0.1 | < 0.1 | < 0.1 | < 0.1 | < 0.1 |

broad volume of the small cortical tissues with E fields amplitudes higher than few $V m^{-1}$.

Figure 5, similarly to previous figure 3, shows the descriptive statistics of E field distributions in subcortical tissues. It shows that in all the tissue where the MENPs are positioned (figures 5(a) and (b)), the maximum E field reaches the activation threshold. Moreover, minima and 75th percentiles are higher than 0.1 and $1 V m^{-1}$, respectively, while

the distribution shape is strongly correlated with the volume of the tissues. Also in these deep structures, an increasing number of MENPs clusters results in increasing volume of stimulated tissue. Conversely, FoE, as suggested by both the example of figure 4 and the descriptive statistics in figure 5(c), can induce at most few $V m^{-1}$ in the subcortical regions, making rather difficult an effective stimulation of these structures.

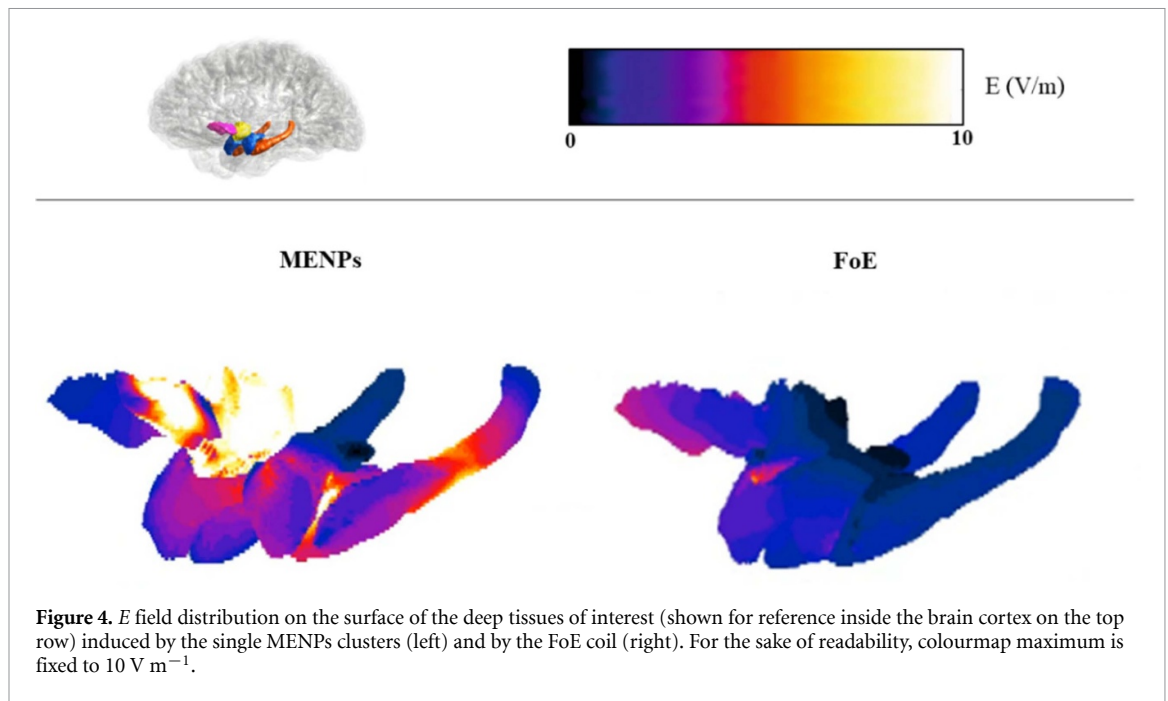


Figure 4. E field distribution on the surface of the deep tissues of interest (shown for reference inside the brain cortex on the top row) induced by the single MENPs clusters (left) and by the FoE coil (right). For the sake of readability, colourmap maximum is fixed to 10 V m^{-1} .

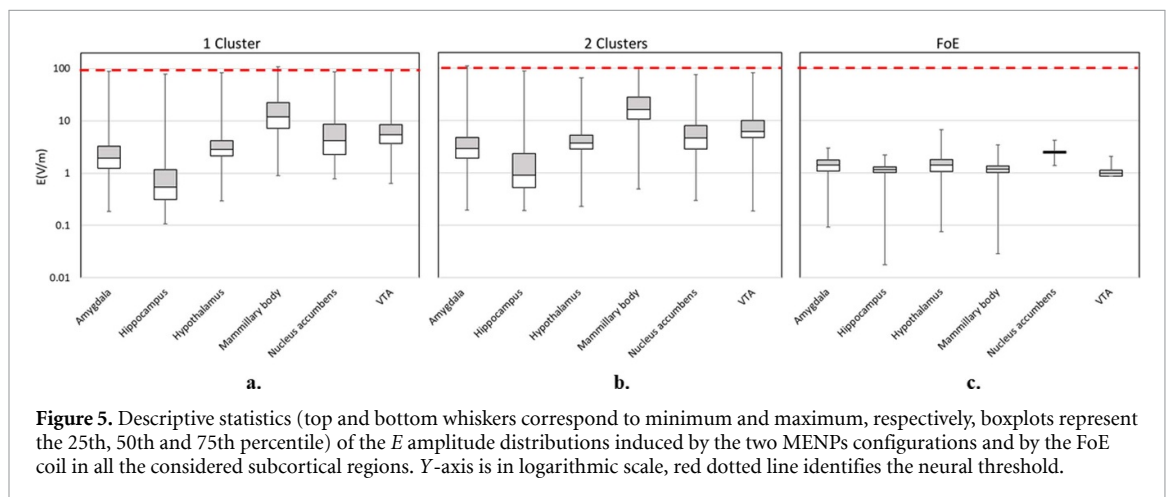


Figure 5. Descriptive statistics (top and bottom whiskers correspond to minimum and maximum, respectively, boxplots represent the 25th, 50th and 75th percentile) of the E amplitude distributions induced by the two MENPs configurations and by the FoE coil in all the considered subcortical regions. Y-axis is in logarithmic scale, red dotted line identifies the neural threshold.

However, median and 75th percentiles range between 1 and 10 V m^{-1} in each tissue of interest, with values depending not only on the tissue volume but also on the distance from the stimulating coil. Also for the deep brain regions, the observed differences between the E amplitude distributions obtained by MENPs clusters and FoE are confirmed as statistically significant by the Kruskal–Wallis test.

The different behaviour of the two stimulation strategies are further suggested by the V_x reported in table 3, showing that FoE can induce E fields up to 1 V m^{-1} over the 80% of the volume of all subcortical tissues (except VTA) but cannot induce E field higher than 1 V m^{-1} in a volume larger than the 0.1% of each tissue. On the contrary MENPs clusters show a strong capability to produce high field levels in their proximity, resulting in not negligible ($>0.1\%$) likely stimulated volumes, especially in the smallest tissues.

4. Discussion

In recent years, there has been a growing interest in exploring novel principles as well as in optimizing existent approaches for brain stimulation.

Among the latter, TMS has been acknowledged as an effective and non-invasive tool for the treatment of several neuropsychiatric disorders, for which the pharmacological treatment is ineffective or bad tolerated. In parallel, recent advancements in neuropsychology, biochemistry, neuroimaging, and experimental studies have revealed that those neuropsychiatric conditions are unlikely to be linked to a single brain region dysfunction (Sampath *et al* 2017). Rather, the evolution of these diseases involves a complex reward circuit alteration affecting integrated pathways, namely the reward system (Russo and Nestler 2013). The main component of this circuit is

Table 3. Percentage volume of each subcortical tissue with E amplitude higher than 1%, 10%, 50% and 70% (V1, V10 V50, V70, respectively) of the maximum amplitude of E in the PFC for each stimulation configuration. Legend: ‘Amy’: Amygdala; Hippo: Hippocampus; Hypo: Hypothalamus; ‘MB’: Mammillary Body; ‘NA’: nucleus accumbens; ‘VTA’: Ventral Tegmental Area.

| | | Amy | Hippo | Hypo | MB | NA | VTA |
|-----------|-----|-------|-------|------|------|------|------|
| 1 Cluster | V1 | 84.9 | 28.6 | 99.8 | 100 | 99.6 | 99.6 |
| | V10 | 5.8 | 3.2 | 6.0 | 57.8 | 21.3 | 19.6 |
| | V50 | 0.4 | 0.2 | 0.6 | 5.8 | 1.3 | 1.0 |
| | V70 | < 0.1 | < 0.1 | 0.2 | 2.0 | 0.2 | 0.2 |
| 2 Cluster | V1 | 99.1 | 45.8 | 100 | 100 | 100 | 100 |
| | V10 | 8.3 | 4.0 | 9.8 | 79.3 | 19.4 | 25.3 |
| | V50 | 0.4 | 0.1 | 0.4 | 7.4 | 1.0 | 1.1 |
| | V70 | < 0.1 | < 0.1 | <0.1 | 1.3 | <0.1 | <0.1 |
| FoE | V1 | 80.3 | 77.3 | 79.9 | 78.5 | 100 | 47.1 |
| | V10 | < 0.1 | < 0.1 | <0.1 | <0.1 | <0.1 | <0.1 |
| | V50 | < 0.1 | < 0.1 | <0.1 | <0.1 | <0.1 | <0.1 |
| | V70 | < 0.1 | < 0.1 | <0.1 | <0.1 | <0.1 | <0.1 |

the mesolimbic dopaminergic pathway, which originates from the ventral tegmental area and projects to PFC towards nucleus accumbens, amygdala, hippocampus, cingulate cortex (O’Reardon *et al* 2007).

Consequently, late efforts to optimize TMS treatments are directed to adequately target these tissues. In this context, computational studies represent an efficient strategy to assess the electric field distributions induced by this technique, contributing also to the interpretation of the therapeutic outcomes. In this modelling study, the capability of traditional FoE to produce a broad electric field distribution over the PFC (see figures 2, 3(d) and table 2) has been confirmed, for example inducing electric field levels higher than tens $V\ m^{-1}$ in a large part of the DLPFC. As expected, due to the intrinsic physics behind TMS, E field amplitude rapidly decays with the distance from the peak in the cortex, resulting in a likely reduced stimulation of insula and cingulate cortex and a dramatic attenuation of E field amplitude in the subcortical and deep tissues (see figures 4, 5(c) and table 3). In order to reduce this decrease, specific deep TMS coils have been proposed (Roth *et al* 2002, Zangen *et al* 2005) and in parallel comparative computational studies (Guadagnin *et al* 2016, Parazzini *et al* 2017) have assessed their effective capability to induce E field levels up to $30\ V\ m^{-1}$ in the same tissues as here considered. These fields are not far from the threshold of neural activation, and are even more close to the threshold for the stimulation of cortical neurons estimated by taking into account the strength-duration curve (Kowalski *et al* 2002). Moreover, they have been proven as effective in activating cortical neurons (Komssi *et al* 2007) as well as hippocampal population of neurons (Jefferys 1981, Ghai *et al* 2000) thus suggesting a possible explanation to the positive outcomes of clinical studies which used deep TMS coils. However, the scarce spatial resolution of traditional TMS and, even more, of deep TMS, together with their scarce energy transmission efficiency are still serious challenges to overcome.

The strategy based on MENPs administration and activation here proposed, can be used to overcome these constraints, having in principle an efficient energy transfer and an elevated spatial resolution. Results of this study show indeed the capability of MENPs clusters, whatever their number, with an induced surface potential of about 100 mV and a ME coefficient $\alpha = 0.0155\ V\ cm^{-1}\ Oe^{-1}$ to induce electric field levels equals to the neuronal activation threshold (i.e. $100\ V\ m^{-1}$) with a spatial resolution of 0.2–0.4 mm, in all the target tissues here considered. This surface potential is close to what measured in the few and recent studies which have successfully used $CoFe_2O_4$ – $BaTiO_3$ MENPs agglomerates in biomedical applications (Betal *et al* 2016, Kozielski *et al* 2021), where surface potential equals to 25–65 mV have been measured as a result of alternating magnetic field of few mT. Consequently, by slightly increasing the external magnetic field or by improving materials properties in line with the recent claims of ME coefficient values above $1\ V\ cm^{-1}\ Oe^{-1}$ (i.e. $1.25\ V\ A^{-1}$) (Palneedi *et al* 2016, Wang *et al* 2020), E fields even two orders of magnitude higher than the ones here reported can be expected.

In this regard, one should also consider different factors still not completely understood and characterized in the interaction between electric stimulation and neural activity. It is known indeed as neuron activation threshold is variable across cell types and cortical layers (Komarov *et al* 2019) and varies according to the temporal features of the stimulus (i.e. the strength-duration curve (Tehovnik *et al* 2006)). Micro-stimulation and retina stimulation studies (Matteucci *et al* 2013, Urdaneta *et al* 2021) have shown that an effective spread of neural activation can be expressed as the square root of the current injected in the electrode divided by the square root of the excitability constant, i.e. $r = (I/K)^{1/2}$, where I is the current level (in μA) r is distance (in millimetres), and K is the excitability constant (in $\mu A\ mm^{-2}$). This last quantity in case of pyramidal neurons, that are the

primary excitation units of most of tissues here considered (e.g. PFC, hippocampus, amygdala), is equal to $1292 \mu\text{A mm}^{-2}$ and then, according to our estimates (i.e. current density over the cluster surface correspond to an injected current of 0.3 mA), produces a spread of activation of about 0.5 mm in all tissues considered. This resolution therefore agrees with our analysis of results and suggests an improvement of at least one order of magnitude over TMS resolution. This reinforces the potential advantages of using MENPs rather than TMS, particularly for the stimulation of deeper tissues. Moreover, the near-DC frequency to which MENPs are characterized and used could make them not only effective in electrically modulating and stimulating neurons at lower electric intensities (Kowalski *et al* 2002), but also eventually lowering the risk of tissue damage and decreasing energy consumption (Wang *et al* 2020).

Along with these considerations, it is important to note that *in vivo* studies in rodents already suggested the absence of MENPs toxicity with no any apparent inflammatory response in mice, both when the nanoparticles are intravenously injected and stereotactically administered in deeper tissues (Kaushik *et al* 2016, Kozielski *et al* 2021, Nguyen *et al* 2021), thus paving the way towards their potential translation in humans. In line with these considerations, our approximated evaluation of safety issues performed according to both magnetic and electric stimulation safety criterion suggests that the use of MENPs not likely would cause tissue damage. In particular, the Brezovich criterion (Brezovich and Meredith 1989), which account for high magnetic field intensity applied for long time, is largely satisfied for the magnetic stimulation protocol here hypothesized (i.e. 140 Hz, <300 mT). Moreover, the eventual local temperature increase due to Joule heating at the MENPs implantation sites could eventually contribute to favour the heat mediated central nervous system (CNS) activation (Odutola *et al* 2018).

As to the direct electric stimulation effects, we have evaluated the charge per phase and the charge density per phase over the MENPs cluster and proven that the combination of these two quantities stays in the area of non-damaging levels of electrical stimulation delimited by Shannon equation (McCreery *et al* 1990).

Interestingly, the significant differences in the E amplitude distributions (figures 3 and 5) here observed varying the number of MENPs clusters, suggest a possible strategy to stimulate a specific tissue volume, by properly tailoring the MENPs dose and preventing the likely unnecessary and unwanted implant of MENPs in multiple sites.

Moreover, the high spatial resolution of E provided by the MENPs activation, as reported in tables 2 and 3, suggests the possibility to design novel electrostimulation selective patterns by opportunely arranging their distributions in predefined target

locations. To this purpose it has recently shown (Guduru *et al* 2018) as MENPs can be used for wirelessly monitor electric field activity of the brain at the sub-neuronal level in real time. This, once guided MENPs in deep tissue by specific timed and sequence of magnetic field gradients (Nair *et al* 2013), open the possibility to create a new strategy for mapping impaired circuits and restore their activity at the same time.

In line with this, future studies will be addressed to investigate by computational techniques the possibility of using MENPs in stimulating neural networks involved in other neurological diseases, such as Parkinson and Alzheimer disease, for which the use of non-invasive approaches coupled with a high-resolution stimulation technique, could offer a substantial improvement (Vissani *et al* 2020).

5. Conclusions

This study focused on the modelling of E amplitude distributions induced by novel proposed MENPs for brain stimulation. The results, in comparison to the traditional non-invasive stimulation technique, i.e. TMS, suggest the use of MENPs to stimulate selectively cortical and subcortical tissues. MENPs therefore could arguably be a promising nanostructure for applications in which a high spatial resolution at cost of minimal invasiveness is required.

Data availability statement

The data that support the findings of this study are available upon reasonable request from the authors.

Acknowledgments

The authors wish to thank ZMT Zurich MedTech AG (www.zmt.swiss) for having provided the simulation software SIM4Life.

ORCID iDs

Serena Fiocchi  <https://orcid.org/0000-0002-6568-8841>

Emma Chiamello  <https://orcid.org/0000-0003-2503-4779>

Alessandra Marrella  <https://orcid.org/0000-0001-6338-5700>

Marta Bonato  <https://orcid.org/0000-0002-5941-297X>

Marta Parazzini  <https://orcid.org/0000-0001-9008-7530>

Paolo Ravazzani  <https://orcid.org/0000-0003-0282-3329>

References

Ali A, Zafar H, Zia M, Ul Haq I, Phull A R, Ali J S and Hussain A 2016 Synthesis, characterization, applications, and

- challenges of iron oxide nanoparticles *Nanotechnol. Sci. Appl.* **9** 49–67
- Bak M, Girvin J P, Hambrecht F T, Kufta C V, Loeb G E and Schmidt E M 1990 Visual sensations produced by intracortical microstimulation of the human occipital cortex *Med. Biol. Eng. Comput.* **28** 257–9
- Banik B L, Fattahi P and Brown J L 2016 Polymeric nanoparticles: the future of nanomedicine *WIREs Nanomed. Nanobiotechnol.* **8** 271–99
- Barbu E, Molnár É, Tsibouklis J and Górecki D C 2009 The potential for nanoparticle-based drug delivery to the brain: overcoming the blood–brain barrier *Expert Opin. Drug Deliv.* **6** 553–65
- Bayda S, Adeel M, Tuccinardi T, Cordani M and Rizzolio F 2019 The history of nanoscience and nanotechnology: from chemical–physical applications to nanomedicine *Molecules* **25** 112
- Betal S, Shrestha B, Dutta M, Cotica L F, Khachatryan E, Nash K, Tang L, Bhalla A S and Guo R 2016 Magneto-elasto-electroporation (MEEP): *in-vitro* visualization and numerical characteristics *Sci. Rep.* **6** 32019
- Brezovich I A and Meredith R F 1989 Practical aspects of ferromagnetic thermoseed hyperthermia *Radiol. Clin. North Am.* **27** 589–602
- Brunoni A R et al 2019 Noninvasive brain stimulation in psychiatric disorders: a primer *Braz. J. Psychiatry* **41** 70–81
- Chen X-Z et al 2017 Hybrid magneto-electric nanowires for nanorobotic applications: fabrication, magneto-electric coupling, and magnetically assisted *in vitro* targeted drug delivery *Adv. Mater.* **29** 1605458
- Danner N, Könönen M, Säisänen L, Laitinen R, Mervala E and Julkunen P 2012 Effect of individual anatomy on resting motor threshold—computed electric field as a measure of cortical excitability *J. Neurosci. Methods* **203** 298–304
- Demirtas-Tatlidede A, Vahabzadeh-Hagh A M and Pascual-Leone A 2013 Can noninvasive brain stimulation enhance cognition in neuropsychiatric disorders? *Neuropharmacology* **64** 566–78
- Deng Z-D, Lisanby S H and Peterchev A V 2013 Electric field depth–focality tradeoff in transcranial magnetic stimulation: simulation comparison of 50 coil designs *Brain Stimul.* **6** 1–13
- Deng Z-D, Lisanby S H and Peterchev A V 2014 Coil design considerations for deep transcranial magnetic stimulation *Clin. Neurophysiol.* **125** 1202–12
- Devan R S and Chougule B K 2007 Effect of composition on coupled electric, magnetic, and dielectric properties of two phase particulate magneto-electric composite *J. Appl. Phys.* **101** 014109
- Eerenstein W, Mathur N D and Scott J F 2006 Multiferroic and magneto-electric materials *Nature* **442** 759–65
- Fiebig M 2005 Revival of the magneto-electric effect *J. Phys. D: Appl. Phys.* **38** R123–52
- Fiocchi S, Chiaramello E, Luzi L, Ferrulli A, Bonato M, Roth Y, Zangen A, Ravazzani P and Parazzini M 2018 Deep transcranial magnetic stimulation for the addiction treatment: electric field distribution modeling *IEEE J. Electromagn. RF Microw. Med. Biol.* **2** 242–8
- Ghai R S, Bikson M and Durand D M 2000 Effects of applied electric fields on low-calcium epileptiform activity in the CA1 region of rat hippocampal slices *J. Neurophysiol.* **84** 274–80
- Goetz L H and Schork N J 2018 Personalized medicine: motivation, challenges, and progress *Fertil. Steril.* **109** 952–63
- Golovin Y I, Gribanovsky S L, Golovin D Y, Zhigachev A O, Klyachko N L, Majouga A G, Sokolsky M and Kabanov A V 2017 The dynamics of magnetic nanoparticles exposed to non-heating alternating magnetic field in biochemical applications: theoretical study *J. Nanopart. Res.* **19** 59
- Gorelick D A, Zangen A and George M S 2014 Transcranial magnetic stimulation in the treatment of substance addiction: TMS as addiction treatment *Ann. New York Acad. Sci.* **1327** 79–93
- Grössinger R, Duong G V and Sato-Turtelli R 2008 The physics of magneto-electric composites *J. Magn. Magn. Mater.* **320** 1972–7
- Guadagnin V, Parazzini M, Fiocchi S, Liorni I and Ravazzani P 2016 Deep transcranial magnetic stimulation: modeling of different coil configurations *IEEE Trans. Biomed. Eng.* **63** 1543–50
- Guduru R, Liang P, Hong J, Rodzinski A, Hadjikhani A, Horstmyer J, Levister E and Khizroev S 2015 Magneto-electric ‘spin’ on stimulating the brain *Nanomedicine* **10** 2051–61
- Guduru R, Liang P, Runowicz C, Nair M, Atluri V and Khizroev S 2013 Magneto-electric nanoparticles to enable field-controlled high-specificity drug delivery to eradicate ovarian cancer cells *Sci. Rep.* **3** 2953
- Guduru R, Liang P, Yousef M, Horstmyer J and Khizroev S 2018 Mapping the brain’s electric fields with magneto-electric nanoparticles *Bioelectron. Med.* **4** 10
- Harnsberger H R and Macdonald A J (eds) 2006 *Diagnostic and Surgical Imaging Anatomy: Brain, Head & Neck, Spine* 1st edn (Salt Lake City, UT: Amirsys)
- Hu J-M, Duan C-G, Nan C-W and Chen L-Q 2017 Understanding and designing magneto-electric heterostructures guided by computation: progresses, remaining questions, and perspectives *npj Comput. Mater.* **3** 18
- Iacono M I et al 2015 MIDA: a multimodal imaging-based detailed anatomical model of the human head and neck *PLoS One* **10** e0124126
- IT²S Foundation 2018 Tissue properties database V4.0 (<https://doi.org/10.13099/VIP21000-04-0>)
- Jefferys J G 1981 Influence of electric fields on the excitability of granule cells in guinea-pig hippocampal slices *J. Physiol.* **319** 143–52
- Johnson M D et al 2013 Neuromodulation for brain disorders: challenges and opportunities *IEEE Trans. Biomed. Eng.* **60** 610–24
- Kaushik A et al 2016 Magnetically guided central nervous system delivery and toxicity evaluation of magneto-electric nanocarriers *Sci. Rep.* **6** 25309
- Kaushik A, Nikkhah-Moshaie R, Sinha R, Bhardwaj V, Atluri V, Jayant R D, Yndart A, Kateb B, Pala N and Nair M 2017 Investigation of AC-magnetic field stimulated nanoelectroporation of magneto-electric nano-drug-carrier inside CNS cells *Sci. Rep.* **7** 45663
- Kolishetti N, Vashist A, Arias A Y, Atluri V, Dhar S and Nair M 2022 Recent advances, status, and opportunities of magneto-electric nanocarriers for biomedical applications *Mol. Asp. Med.* **83** 101046
- Komarov M, Malerba P, Golden R, Nunez P, Halgren E and Bazhenov M 2019 Selective recruitment of cortical neurons by electrical stimulation *PLoS Comput. Biol.* **15** e1007277
- Komssi S, Savolainen P, Heiskala J and Kähkönen S 2007 Excitation threshold of the motor cortex estimated with transcranial magnetic stimulation electroencephalography *NeuroReport* **18** 13–16
- Kopyl S, Surmenev R, Surmeneva M, Fetisov Y and Kholkin A 2021 Magneto-electric effect: principles and applications in biology and medicine—a review *Mater. Today* **12** 100149
- Kowalski T, Silny J and Buchner H 2002 Current density threshold for the stimulation of neurons in the motor cortex area *Bioelectromagnetics* **23** 421–8
- Kozielski K L, Jahanshahi A, Gilbert H B, Yu Y, Erin Ö, Francisco D, Alosaimi F, Temel Y and Sitti M 2021 Nonresonant powering of injectable nanoelectrodes enables wireless deep brain stimulation in freely moving mice *Sci. Adv.* **7** eabc4189
- Lee S and Jun B-H 2019 Silver nanoparticles: synthesis and application for nanomedicine *Int. J. Mol. Sci.* **20** 865
- Liu X-M, Fu S-Y and Huang C-J 2005 Synthesis and magnetic characterization of novel CoFe₂O₄–BiFeO₃ nanocomposites *Mater. Sci. Eng. B* **121** 255–60

- Loo C K and Mitchell P B 2005 A review of the efficacy of transcranial magnetic stimulation (TMS) treatment for depression, and current and future strategies to optimize efficacy *J. Affective Disorders* **88** 255–67
- Matteucci P B, Chen S C, Tsai D, Dodds C W D, Dokos S, Morley J W, Lovell N H and Suaning G J 2013 Current steering in retinal stimulation via a quasimonopolar stimulation paradigm *Investigative Ophthalmol. Vis. Sci.* **54** 4307
- McCreery D B, Agnew W F, Yuen T G H and Bullara L 1990 Charge density and charge per phase as cofactors in neural injury induced by electrical stimulation *IEEE Trans. Biomed. Eng.* **37** 996–1001
- McIntyre C C, Mori S, Sherman D L, Thakor N V and Vitek J L 2004 Electric field and stimulating influence generated by deep brain stimulation of the subthalamic nucleus *Clin. Neurophysiol.* **115** 589–95
- Nagesetti A et al 2017 Multiferroic coreshell magnetoelectric nanoparticles as NMR sensitive nanoprobe for cancer cell detection *Sci. Rep.* **7** 1610
- Nair M, Guduru R, Liang P, Hong J, Sagar V and Khizroev S 2013 Externally controlled on-demand release of anti-HIV drug using magneto-electric nanoparticles as carriers *Nat. Commun.* **4** 1707
- Nguyen T, Gao J, Wang P, Nagesetti A, Andrews P, Masood S, Vriesman Z, Liang P, Khizroev S and Jin X 2021 *In vivo* wireless brain stimulation via non-invasive and targeted delivery of magnetoelectric nanoparticles *Neurotherapeutics* **18** 2091–106
- O'Reardon J P et al 2007 Efficacy and safety of transcranial magnetic stimulation in the acute treatment of major depression: a multisite randomized controlled trial *Biol. Psychiatry* **62** 1208–16
- Odutola T, Myrovali E, Makridis A, Maniotis N, Angelakeris M, Kimiskidis V and Samaras T 2018 Can magnetic nanoparticles thermally assist the beneficiary role of transcranial magnetic stimulation? 2018 EMF-Med 1st World Conf. on Biomedical Applications of Electromagnetic Fields (EMF-MED) (Split: IEEE) pp 1–2
- Palneedi H, Annareddy V, Priya S and Ryu J 2016 Status and perspectives of multiferroic magnetoelectric composite materials and applications *Actuators* **5** 9
- Parazzini M, Fiocchi S, Chiaramello E, Roth Y, Zangen A and Ravazzani P 2017 Electric field estimation of deep transcranial magnetic stimulation clinically used for the treatment of neuropsychiatric disorders in anatomical head models *Med. Eng. Phys.* **43** 30–38
- Pelaz B et al 2017 Diverse applications of nanomedicine *ACS Nano* **11** 2313–81
- Regenold W T, Deng Z-D and Lisanby S H 2022 Noninvasive neuromodulation of the prefrontal cortex in mental health disorders *Neuropsychopharmacology* **47** 361–72
- Rodriguez M, Kaushik A, Lapierre J, Dever S M, El-Hage N and Nair M 2017 Electro-magnetic nano-particle bound Beclin1 siRNA crosses the blood–brain barrier to attenuate the inflammatory effects of HIV-1 infection *in vitro J. Neuroimmune Pharmacol.* **12** 120–32
- Roth Y, Padberg F and Zangen A 2007 Transcranial magnetic stimulation of deep brain regions: principles and methods *Advances in Biological Psychiatry* ed M A Marcolin and F Padberg (Basel: Karger) pp 204–24
- Roth Y, Zangen A and Hallett M 2002 A coil design for transcranial magnetic stimulation of deep brain regions *J. Clin. Neurophysiol.* **19** 361–70
- Russo S J and Nestler E J 2013 The brain reward circuitry in mood disorders *Nat. Rev. Neurosci.* **14** 609–25
- Ryan C N M, Doulgkeroglou M N and Zeugolis D I 2021 Electric field stimulation for tissue engineering applications *BMC Biomed Eng.* **3** 1
- Sampath D, Sathyanesan M and Newton S 2017 Cognitive dysfunction in major depression and Alzheimer's disease is associated with hippocampus–prefrontal cortex dysconnectivity *Neuropsychiatr. Dis. Treat.* **13** 1509–19
- Singer A et al 2020 Magnetoelectric materials for miniature, wireless neural stimulation at therapeutic frequencies *Neuron* **107** 631–43.e5
- Stewart T S et al 2018 Magnetoelectric nanoparticles for delivery of antitumor peptides into glioblastoma cells by magnetic fields *Nanomedicine* **13** 423–38
- Stimphil E, Nagesetti A, Guduru R, Stewart T, Rodzinski A, Liang P and Khizroev S 2017 Physics considerations in targeted anticancer drug delivery by magnetoelectric nanoparticles *Appl. Phys. Rev.* **4** 021101
- Tehovnik E J, Tolias A S, Sultan F, Slocum W M and Logothetis N K 2006 Direct and indirect activation of cortical neurons by electrical microstimulation *J. Neurophysiol.* **96** 512–21
- Urdaneta M E, Kunigk N G, Delgado F, Fried S I and Otto K J 2021 Layer-specific parameters of intracortical microstimulation of the somatosensory cortex *J. Neural Eng.* **18** 055007
- Vissani M, Isaias I U and Mazzoni A 2020 Deep brain stimulation: a review of the open neural engineering challenges *J. Neural Eng.* **17** 051002
- Wang P et al 2020a Colossal magnetoelectric effect in core–shell magnetoelectric nanoparticles *Nano Lett.* **20** 5765–72
- Wang Z-X, Feng Z-Y, Zheng L-P and Yuan Y 2020b Sinusoidal stimulation on afferent fibers modulates the firing pattern of downstream neurons in rat hippocampus *J. Integr. Neurosci.* **19** 413
- Xie J, Chen K, Lee H-Y, Xu C, Hsu A R, Peng S, Chen X and Sun S 2008 Ultrasmall c(RGDyK)-coated Fe₃O₄ nanoparticles and their specific targeting to integrin $\alpha_v\beta_3$ -rich tumor cells *J. Am. Chem. Soc.* **130** 7542–3
- Yue K, Guduru R, Hong J, Liang P, Nair M and Khizroev S 2012 Magneto-electric nano-particles for non-invasive brain stimulation *PLoS One* **7** e44040
- Zangen A, Roth Y, Voller B and Hallett M 2005 Transcranial magnetic stimulation of deep brain regions: evidence for efficacy of the H-coil *Clin. Neurophysiol.* **116** 775–9